HHS Public Access

Author manuscript

Hear Res. Author manuscript; available in PMC 2019 May 08.

Published in final edited form as:

Hear Res. 2019 May ; 376: 11–21. doi:10.1016/j.heares.2018.11.002.

Tonotopy in calcium homeostasis and vulnerability of cochlear hair cells

Robert Fettiplace[1,*] and **Jong-Hoon Nam**[2]

[1]Department of Neuroscience, University of Wisconsin, Madison, WI 53706

[2]Departments of Mechanical Engineering and Biomedical Engineering, University of Rochester, Rochester, NY 14627

Abstract

Ototoxicity, noise overstimulation, or aging, can all produce hearing loss with similar properties, in which outer hair cells (OHCs), principally those at the high-frequency base of the cochlea, are preferentially affected. We suggest that the differential vulnerability may partly arise from differences in Ca^{2+} balance among cochlear locations. Homeostasis is determined by three factors: Ca^{2+} influx mainly via mechanotransducer (MET) channels; buffering by calcium-binding proteins and organelles like mitochondria; and extrusion by the plasma membrane CaATPase pump. We review quantification of these parameters and use our experimentally-determined values to model changes in cytoplasmic and mitochondrial Ca^{2+} during Ca^{2+} influx through the MET channels. We suggest that, in OHCs, there are two distinct micro-compartments for Ca^{2+} handling, one in the hair bundle and the other in the cell soma. One conclusion of the modeling is that there is a tonotopic gradient in the ability of OHCs to handle the Ca^{2+} load, which correlates with their vulnerability to environmental challenges. High-frequency basal OHCs are the most susceptible because they have much larger MET currents and have smaller dimensions than low-frequency apical OHCs.

Keywords

calcium; hearing loss; mechanotransducer channels; mitochondria; PMCA2 calcium pump; stereociliary bundle

Introduction

Sound stimuli are detected by vibrations of the stereociliary (hair) bundles on cochlear hair cells, and the electrical signals generated are then relayed via synapses onto auditory nerve terminals. Most hearing loss is attributable to damage to the sensory cells through a variety of genetic or environmental causes. Genetic deafness arises from mutations that mainly affect hair cell function, and it accounts for about one child in 500 born profoundly deaf or becoming so before adulthood (Dror et al., 2010; Vona et al., 2015). More than 50 different

[*]To whom correspondence should be addressed at: 185 Medical Sciences Building, 1300 University Avenue, Madison, WI 53706, USA, Tel: 608-262-9320., fettiplace@wisc.edu.

The authors declare they have no competing interests.

genes have presently been linked to hearing loss and, for each, protein malfunction due to a point mutation can be sufficient to cause deafness. For autosomal recessive hearing loss, the six most common causative genes, in order of frequency, are *GJB2*, *SLC26A4*, *MYO15A*, *OTOF, CDH23* and *TMC1* (Hilgert et al., 2009). Three of these, *MYO15A* (Liang et al., 1999), *CDH23* (Bork et al., 2001), and *TMC1* (Kurima et al., 2002) code for hair bundle proteins. *TMC1* encodes transmembrane channel-like protein 1 (TMC1) which is thought to be a component of the mechanotransducer (MET) channel (Fettiplace, 2016; Kawashima et al., 2011). Many of the deafness genes were first identified from human mutations, but the location and role of the corresponding proteins were subsequently explored from equivalent mutations in mice (Michalski et al., 2015).

Hearing loss can also stem from a variety of environmental insults. These include: (i) ototoxicity as a side-effect of drugs such as aminoglycoside antibiotics (Alharazneh et al., 2011; Ryan et al., 1980), or the chemotherapeutic agent cis-platin (Sheth et al., 2017); (ii) acoustic trauma evoked by loud or prolonged noise (Liberman, 2016; Liberman et al., 1978); and (iii) age-dependent deterioration, usually referred to as presbycusis (Cruickshanks et al., 1998; Jayakody et al., 2018). The distinction between genetic and environmental etiologies is not firm, as there are genetic modifiers of both presbycusis (Gates et al., 1999) and aminoglycoside ototoxicity (Cortopassi et al., 1994). A common factor with all three forms of environmentally-induced deafness is that they primarily target the cochlear outer hair cells (OHCs), rather than the inner hair cells (IHCs) (Fig. 1). This selectivity towards OHCs was especially apparent after treatment with aminoglycoside antibiotics such as kanamycin, prolonged treatment with which produced OHC degeneration and substantial threshold elevation (Ryan et al., 1980). The selective effects of kanamycin were used to conclude that OHCs are responsible for high sensitivity and sharp frequency tuning of the auditory periphery (Dallos et al., 1978; Kiang et al., 1986), properties distinct from IHCs, which transmit the acoustic signals via synapses on auditory nerve terminals. It was later demonstrated that the unique property of OHCs to mechanically amplify the acoustic input by force generation stems from the piezoelectric protein prestin present at high density in their lateral membranes (Dallos et al., 2008; Zheng et al., 2000). Oscillations in OHC membrane potential elicit contraction or elongation of these cylindrical cells. OHCs and IHCs thus perform disparate roles in the cochlea, and to match this separation of function, they have distinct morphology and electrophysiological characteristics as discussed below. However, the greater susceptibility of OHCs to otoxocity or other environmental effects suggests they have unusual physiological characteristics.

A second generalization about environmental insults to the auditory system is that OHCs in the high-frequency region of the cochlea are the most vulnerable, and first to degenerate. The long coiled structure of the cochlea is arranged tonotopically, so each tone frequency has a place of maximal sensitivity along the organ. Thus, death of hair cells in the basal turn lead to high-frequency hearing loss. This tonotopic susceptibility is the case with aminoglycoside antibiotic ototoxicity (Ryan et al., 1980), exposure to broad-band noise (Liberman et al., 1978) and presbycusis (Cruickshanks et al., 1998). Elderly people commonly have high-frequency hearing loss. These observations raise several related questions. Why are OHCs more vulnerable to environmental insults, and why is there a tonotopic gradient in degeneration from high-frequency to low-frequency OHCs? Because of

some ambiguities in use of the terms apex and base, we shall subsequently refer to the 'base' as the high-frequency region, and the 'apex' as the low-frequency region. Is there a common factor with all environmental assaults culminating in apoptosis of high-frequency OHCs? It should be cautioned however that there can be similar manifestations with deafness of genetic origin, especially those affecting hair cell mechanotransduction. For example, high-frequency OHCs are the first to degenerate with *TMC1* mutations (Kawashima et al., 2011; Vreugde et al., 2002).

The aim of the review is to address these questions by offering the hypothesis that intracellular Ca^{2+} homeostasis may be a contributory factor making OHCs, especially those in the high-frequency region of the cochlea, most vulnerable to environmental assault (Mammano, 2011). In the following sections, each of the factors dictating Ca^{2+} distribution will be quantified and will be incorporated into a theoretical model for predicting Ca^{2+} homeostasis. Important players to be considered are the mitochondria, which perform a key role in many cell functions including regulation of Ca^{2+} signaling. Prolonged increase in intra-mitochondrial Ca^{2+} concentration can lead to opening of the mitochondrial permeability transition pore (Morciano et al., 2015), a critical event that culminates in cell death by apoptosis (Rizzuto et al., 2012). This review does not address 'hidden hearing loss' which is thought to stem from the environmental effects such as noise on the synaptic function of IHCs (Liberman, 2016).

Calcium homeostasis in hair cells – a summary

The cytoplasmic concentration of Ca^{2+} in most cells is held at ~100 nM, determined in the long term as the balance between two factors, the rates of influx and of efflux of the ion. For the hair cell, the principal routes of entry are through Ca^{2+} permeable MET channels in the hair bundle (Beurg et al., 2006; Ohmori, 1985) and voltage-sensitive Ca^{2+} (Cav1.3) channels around the basolateral aspect of the hair cells (Brandt et al., 2003). IHCs possess more voltage-sensitive Ca^{2+} channels in order to drive synaptic transmission onto type I afferent terminals. In adult OHCs, there may be only a few Cav1.3 channels regulating synapses onto type II afferents (Knirsch et al., 2007; Weisz et al., 2012), but there are acetylcholine receptors, composed of Ca^{2+}-permeable α9 and α10 subunits, mediating efferent action (Gomez-Casati et al., 2005). Ca^{2+} is extruded solely by a plasma membrane CaATPase. The PMCA2 isoform is highly concentrated in the hair bundle, whereas the PMCA1 isoform may be present in the cell body, especially of IHCs (Chen et al., 2012; Dumont et al., 2001). Factors influencing the spatiotemporal distribution of free Ca^{2+} are more complex, and on a short time scale, there can be cytoplasmic gradients away from the source determined by a variety of calcium buffers (Schwaller, 2010). These buffers may be mobile proteins such as calbindin-D28k, or fixed, including immobile cytoplasmic proteins, as well as organelles like mitochondria and endoplasmic reticulum. An important distinction between the two types of buffer is that mobile buffers augment the diffusion of Ca^{2+} whereas fixed buffers slow it (Zhou et al., 1993). There is little information about the identity of the fixed buffers, though they are thought to have a low affinity for Ca^{2+}. Overall, only about one percent of the Ca^{2+} that enters a cell remains free.

Most is known about the mobile cytoplasmic Ca^{2+}-binding proteins, which are present in significant amounts in both IHCs and OHCs. There are four major mobile Ca^{2+}-binding proteins in cochlear hair cells: calretinin, calbindin-D28k, parvalbumin-α and parvalbumin-β (also known as oncomodulin (Sakaguchi et al., 1998)). These four are generally regarded as buffers rather than intermediates in Ca^{2+} signaling pathways. All display differences between IHCs and OHCs in concentration and Ca^{2+} binding properties (Schwaller, 2010), and also vary along the cochlea (Hackney et al., 2005; Pack et al., 1995). Calmodulin is another calcium-binding protein that is well represented in hair cells (Imamura et al., 1996; Nakazawa, 2001; Pack et al., 1995) and may aid in calcium buffering, but much of it is probably bound to immobilized target proteins, and is involved in signaling. There are also substantial amounts of calreticulin and calnexin, mainly associated with protein folding in the endoplasmic reticulum (Michalak et al., 2009).

While the relative distributions of such proteins are often inferred from immuno-fluorescence intensity, this is a function of the efficacy of the antibody. For example, there is a very efficient antibody for calretinin, which produces bright labeling that does not necessarily reflect a high concentration of the protein. However, protein concentrations can be quantified precisely in electron-microscopical sections, by calibrating immunogold labeling of tissue against gels containing known amounts of the relevant protein (Hackney et al., 2003; Hackney et al., 2005). This technique demonstrates that calretinin and parvalbumin-α have the largest concentrations in IHCs, whereas oncomodulin and calbindin-D28k are most concentrated in OHCs. All except oncomodulin have sub-millimolar concentrations and, taken together, IHCs have about one tenth the concentration of proteinaceous calcium buffers as OHCs. The OHC buffering is dominated by oncomodulin, which is present at 2 to 3 mM, increasing from the low-frequency region to high-frequency region (Hackney et al., 2005). Taking into account that oncomodulin has two Ca^{2+}-binding sites and calbindin-D28k has four, together they are equivalent to 5 mM free Ca^{2+} binding sites in OHCs. The large amount of proteinaceous calcium buffer in OHCs, similar only to the millimolar concentrations of parvalbumin-α in skeletal muscle, is puzzling and implies that Ca^{2+} has an important signaling role in OHCs. In skeletal muscle, large Ca^{2+} transients spread throughout the fiber to initiate the contractile process, and binding of Ca^{2+} by parvalbumin-α is important in facilitating relaxation. The relative amounts of parvalbumin- α in different muscle types are correlated with the relaxation rate (Heizmann et al., 1982), fast twitch muscles having more of the Ca^{2+} binding protein than slow muscles. Fast twitch muscles in parvalbumin-α knock-out mice show prolonged contraction–relaxation cycles (Schwaller et al., 1999). By comparison, targeted knockout of oncomodulin ($Ocm^{-/-}$) in mice causes progressive cochlear dysfunction, OHC degeneration, and up to 80 dB elevation in ABR threshold (Tong et al., 2016). A curious feature of the oncomodulin knockout is the slow development of the degeneration. Thus both morphology and function are normal at one month, and it takes three to four months for the morphology to deteriorate and function to fail.

Routes of Ca^{2+} entry

The major routes of Ca^{2+} entry are via the MET channels and the voltage-sensitive Ca^{2+} channels. There are two pertinent properties of the MET currents in OHCs. Firstly, the

maximum current varies with tonotopically, the amplitude increasing from 1.7 nA at the apical turn to as much 7 nA at the basal turn (Johnson et al., 2011) (Fig. 2). Secondly, under physiological conditions, in which the stereociliary bundles are exposed to endolymph, about half the channels are activated at rest irrespective of location (Fig. 2), thus generating a standing 'silent' current. A large (silent) transducer current is therefore constantly flowing into OHCs. The MET channels show a non-selective cation permeability, with Ca^{2+} being most permeable, about 5 time more permeable than Na+ (Beurg et al., 2006; Ohmori, 1985). High speed imaging has been used to estimate the fraction of the MET current carried by Ca^{2+} as about 0.15 with bundles exposed to perilymph, and 0.002 when exposed to endolymph (Beurg et al., 2010) containing only 20 to 40 μM Ca^{2+} (Gill et al., 1997). From these observations, it is possible to estimate the maximum Ca^{2+} load imposed on the OHCs as ranging from 4 pA at the cochlear low-frequency to 14 pA at the high-frequency region. Accompanying this tonotopic increase in MET current is an opposite gradient in cell size. Thus in all cochleas, the length of the OHCs decreases several-fold from low-frequency to high-frequency (Fettiplace, 2017), causing a related decrease in electrical cell capacitance (Fig. 2). The combined changes in cell capacitance, C_m, and input resistance, R_i, cause a large reduction in membrane time constant (= $C_m.R_i$), which may facilitate prestin activation at high frequencies (Johnson et al., 2011). However, the reduction in cell size has the drawback that Ca^{2+} flowing into a three-fold smaller volume evokes a larger load. This is particularly applicable to the hair bundle, the height of which decreases four-fold from low-frequency to high-frequency (Lim, 1986; Roth et al., 1992). There will be a much larger load of Ca^{2+} entering at the tips of the stereocilia at the high-frequency compared to the low-frequency region of the cochlea.

IHCs differ in the properties of their Ca^{2+} homeostasis compared to OHCs. Firstly, there is little tonotopic gradient in the MET current of IHCs and their MET current amplitude never attains that of high-frequency OHCs (Johnson et al., 2012). Secondly, the resting open probability of the MET channels is less in IHCs than OHCs (Johnson et al., 2011; Johnson et al., 2012), so generating a smaller standing current. The difference in resting open probability probably stems from the lower concentration of mobile calcium buffer, a consequence previously demonstrated in turtle hair cells (Ricci et al., 1998) and supported by recordings in mammalian cochlear hair cells (Corns et al., 2014). IHCs have a tenth the Ca^{2+} buffer concentration, they have no gradient in MET current amplitude, and the tallest stereocilia have a larger diameter than those in OHC bundles (0.5 μm diameter compared to 0.2 μm), increasing the bundle volume. However, IHCs do possess voltage-sensitive Ca^{2+} channels around the basolateral membrane, but in adult animals, the peak Ca^{2+} current is surprisingly small, only ~100 pA, and, at the resting potential of −60 mV, less than 5 pA will flow (Johnson et al., 2011; Johnson et al., 2012). Nonetheless, this Ca^{2+} flux is still comparable to that produced through the MET channels, though importantly it will be diluted into a large cellular volume invariant with cochlear location. Thus the prediction is that IHCs are likely to have fewer problems in balancing their Ca^{2+} than will OHCs. An indicator of this difference is the smaller complement of CaATPase pumps in the stereociliary bundles of IHCs, as shown by the pump quantification described below. Ca^{2+} influx could in theory also occur in OHCs via the nicotinic acetylcholine receptors at the base of the cell, though it seems likely these will be activated infrequently.

Ca^{2+} efflux via the plasma membrane calcium (PMCA) pump

The two major mechanisms for extruding Ca^{2+} from a cell are the plasma membrane CaATPase pump (PMCA), which hydrolyzes one ATP per Ca^{2+} ion expelled, and the sodium/calcium exchanger, in which three Na^{+} ions enter in exchange for removal of one Ca^{2+} ion. The sodium/calcium exchanger has a higher turnover rate and is employed to extrude Ca^{2+} in many cells including vertebrate photoreceptors (Hodgkin et al., 1987; Yau et al., 1984). In these sensory receptors, the divalent ion enters through the Ca^{2+}-permeable cyclic nucleotide-gated channels and regulates steps in the G-protein-coupled transducer pathway to generate light adaptation (Luo et al., 2008). However, there is no evidence for a sodium/calcium exchanger in cochlear hair cells, which employ only PMCA pumps for extruding Ca^{2+} (Tucker et al., 1995; Yamoah et al., 1998). PMCA2A is the major isoform used in mammalian hair cells (Dumont et al., 2001), and in OHCs it occurs as the spliced PMCAw/a isoform (Hill et al., 2006). The PMCA2 isoform is especially concentrated in the hair bundles of OHCs, and much less so in IHC bundles (Chen et al., 2012; Dumont et al., 2001). However, there is also expression of the PMCA1 isoform in the basolateral membrane of IHCs to extrude Ca^{2+} entering through the voltage-sensitive Ca^{2+} channels. We do not have any estimate of the PMCA1 density. In contrast, immunolabeling for PMCA2 in electron-microscope sections of OHCs shows the pumps are concentrated in the hair bundle, and calibration of the label, using a technique similar to that applied to the Ca^{2+}-binding proteins (Fig. 3), allowed the PMCA density to be determined as ~2200/μm^2 in OHCs, but less than a tenth of that in IHCs (Chen et al., 2012). A similarly high density of PMCA2 pumps was previously observed in frog saccular hair cells associated with a large Ca^{2+} efflux from the hair bundle (Yamoah et al., 1998). Comparison of the pump density with the maximum pump rate inferred from the electrogenic current in OHCs allows the turnover rate of a single PMCA2 monomer to be estimated as 200/sec (Chen et al., 2012), making it a very fast P-type pump isomer. Moreover, despite the apical-basal gradient in cell size and MET current, there is little difference in hair-bundle PMCA2w/a density between apical and basal OHCs. Stereocilia in the high-frequency basal bundles are a quarter the length of those at the apex, about 1.0 μm compared to 4.0 μm (Roth et al., 1992), but possess more stereocilia per bundle, 110 compared to 85 (Beurg et al., 2006), the net effect being fewer PMCA2 pumps per bundle. Null mutations of the *Atp2b2* gene, coding for the PMCA2 pump isoform, are linked to hereditary deafness in both humans (Ficarella et al., 2007) and mice (Kozel et al., 1998; McCullough et al., 2004; Street et al., 1998).

An indication of the importance of the pumps is the deleterious effect of PMCA2 mutations in which the pumping rate is reduced. Some mutations lead to the truncation of the protein product and disappearance of the PMCA2 from the stereocilia of mouse hair cells. In other cases, exemplified by the mouse mutants *Oblivion* (Spiden et al., 2008) and *Tommy* (Bortolozzi et al., 2010), single amino-acid alteration cause a dominant hearing loss. Heterozygotes showed increasing hearing impairment with age, followed by a progressive high-to low-frequency degeneration of OHCs. In both mutants, the protein was correctly targeted to the plasma membrane, but the pump had a reduced capacity to clear the Ca^{2+} from the stereocilia, as estimated by the decay in the divalent ion following flash photolysis of caged Ca^{2+}. Ca^{2+} clearance was 50 per cent slower in both *Oblivion* and *Tommy* than in

wild-type (Bortolozzi et al., 2018). These examples show that progressive hearing loss can result from an imbalance in Ca^{2+} handling, and that high-frequency OHCs are more vulnerable than low-frequency ones.

The endolymph concentration of Ca^{2+}, at 20 – 40 μM (Bosher et al., 1978; Ikeda et al., 1987; Salt et al., 1989), is larger than might be expected from equilibrium considerations. Given a perilymph [Ca^{2+}] of 1.3 mM, and an endolymphatic potential of 100 mV, the predicted endolymph [Ca^{2+}] using the Nernst equation is ~1 μM; the physiological [Ca^{2+}] is 20 fold higher, which is thought to arise by an increase in Ca^{2+} attributable to extrusion from the OHC stereociliary bundles. In the absence of the Ca^{2+} extrusion, it might be expected that the endolymph [Ca^{2+}] will drop. Mutation of PMCA2 in the *dfw2j* isoform caused the pump to be excluded from the stereocilia, and was associated with a lowering of endolymph [Ca^{2+}] from 23 μM in wild-type to 7 μM in *dfw2j* (Wood et al., 2004). This result suggests that Ca^{2+} efflux by PMCA2 pumps in the stereociliary bundle contributes to maintaining an appropriate level of Ca^{2+} in endolymph, which is necessary to optimize mechanotransduction. The bulk [Ca^{2+}] in endolymph has been assayed in a number of preparations as 20 to 40 μM, but the exact concentration in the sub-tectorial space around the tip link might be higher than in the bulk endolymph (Yamoah et al., 1998). Any reduction in Ca^{2+} below the physiological concentration is likely to increase the fragility of the tip link and will eventually undermine transduction. This may provide a clue as to why, both in humans (Ficarella et al., 2007; Schultz et al., 2005) and mice (Noben-Trauth et al., 2003; Watson et al., 2013), PMCA2 mutations potentiate the deafness phenotype induced by co-existing mutations of cadherin-23, a component of the interciliary tip link that transmits force to the MET channel. It is envisaged that even though the tip link structure is preserved in some CDH23 mutations, nevertheless the tip links will become more mechanically brittle, or conserved Ca^{2+}-binding residues will be altered by the mutations (Jaiganesh et al., 2018). Both effects would be exacerbated by reduced endolymph [Ca^{2+}].

The contribution of mitochondria

Mitochondria are the power stations of the cell, generating ATP using the H^+-dependent synthase via the respiratory electron transport chain. During operation of the respiratory chain, H^+ ions are translocated across the inner of the two mitochondrial membranes, thus creating a large proton gradient, and a negative membrane potential of up to −180 mV. Besides production of ATP, mitochondria, by acting as fixed Ca^{2+} buffers, also play a role in Ca^{2+} signaling (Babcock et al., 1997; Brini, 2003; De Stefani et al., 2016). They rapidly take up Ca^{2+} through a recently identified uniporter (Baughman et al., 2011; De Stefani et al., 2011) that allows the divalent to move down its electrochemical gradient into the electronegative matrix. They can also release the divalent ion through two exchangers, a Ca^{2+}/ H^+ exchanger and a Ca^{2+}/ Na^+ exchanger. One other pathway contributing to movement of ions and other solutes across the inner membrane is the permeability transition pore (PTP) (Bernardi et al., 2015). This transporter behaves as non-selective, high-conductance channel, activation of which can cause swelling of the mitochondria, rupture of their outer membrane, and release of caspase co-factors such as cytochrome c into the cytoplasm as a prelude to cell death. Each of the various ion transporters can be identified physiologically by the specific compound that inhibits its activity; e.g., Ruthenium Red

blocks the uniporter, cyclosporin A blocks the PTP, and FCCP dissipates the proton gradient (Babcock et al., 1997).

The mitochondrial uniporter (MCU) drives rapid and massive Ca^{2+} entry, but only at high cytosolic Ca^{2+} concentrations near Ca^{2+} microdomains. Owing to its low affinity for Ca^{2+}, the uniporter requires a high local cytoplasmic [Ca^{2+}] (~10 μM) to function. These calcium microdomains can be generated near Ca^{2+} channels in the plasma membrane and close to the endoplasmic reticulum. Mitochondria in OHCs aggregate beneath the cuticular plate where they might sense the Ca^{2+} that has entered via the MET channels. Changes in mitochondrial Ca^{2+} during cell activity can be monitored with fluorescent dyes, such as Rhod2, which is taken up by the mitochondria (Babcock et al., 1997; David et al., 1998). Application of Rhod2 in rat OHCs showed that during hair bundle deflection, the sub-cuticular plate mitochondria accumulate Ca^{2+} throughout a sustained mechanical stimulus (Fig. 4). The uptake is abolished by dissipation of the H+ gradient with FCCP, which also results in a shift in the MET channel activation curve similar to that resulting from blocking the PMCA2 pump (Beurg et al., 2010). The layer of mitochondria below the cuticular plate effectively acts as firewall, preventing Ca^{2+} that has entered via the MET channels from penetrating deeper into the soma, thereby isolating the hair bundle compartment. Their presence in OHCs (Fig 4), coupled with the large standing and evoked MET currents in these cells, argues that Ca^{2+} metabolism is different in OHCs and IHCs. We suggest that OHCs possess are two distinct micro-compartments with respect to Ca^{2+} homeostasis, one being in the soma and the other in the stereocilia. The latter may resemble the "Ca^{2+} compartment" proposed to exist in dendritic spines and associated with long-term potentiation, whereas the former is analogous to the body of the dendrite (Sabatini et al., 2002; Yuste et al., 2000). For IHCs, the differences between these compartment may be less marked. For both OHCs and IHCs, there is also an accumulation of mitochondria in the sub-nuclear zone in the vicinity of the synaptic apparatus.

A prolonged increase in mitochondrial Ca^{2+} uptake can induce an increase in the respiratory rate and ATP production. But a pathologically large elevation in mitochondrial [Ca^{2+}] can eventually cause a drop in the inner membrane potential, and augment the production of reactive oxygen species (ROS; O_2 −), which may trigger a pathway culminating in apoptosis. This pathway is: Ca^{2+} overload → ROS production → opens PTP → cytochrome C release → activation of caspase 3 → and triggering apoptosis. Brief openings of the permeability transition pore, with subsequent release of small amounts of ROS, may play an important physiological function in maintaining mitochondrial homeostasis by releasing various amounts of ROS. However, at higher levels of ROS, prolonged PTP openings may release a burst of ROS leading to mitochondrial destruction and eventually cell death (Zorov et al., 2014). The hypothesis that increased ROS production is a key factor in various types of sensorineural deafness is an old idea (see review by (Kamogashira et al., 2015)), and has led to a search for antioxidant drugs that might confer some protection. A recent example in humans is that sodium thiosulfate may provide some protection from cis-platin-induced hearing loss (Brock et al., 2018). There is also evidence that aminoglycoside toxicity is linked to ROS production driven by mitochondrial Ca^{2+} uptake, because it can be partially alleviated by blocking the mitochondrial uniporter

(Esterberg et al., 2016). This led to suggestion that agents that prevent mitochondrial oxidation may counter the toxic effects of aminoglycosides (Esterberg et al., 2016)

A model of Ca^{2+} homeostasis.

Based on delineation of the factors involved in hair-cell Ca^{2+} homeostasis, it is possible to simulate the time course and extent of Ca^{2+} changes during an imposed load using the quantitative values available for almost every element in the pathway. These include Ca^{2+} influx via MET channels, diffusion and buffering with oncomodulin, and extrusion by the stereociliary PMCA2 pumps, all of which we have characterized experimentally. For the mitochondrial Ca^{2+} handling, values used previously (Beurg et al., 2010) were assumed, with influx via the uniporter (MCU) and expulsion by a Na+/Ca^{2+} exchanger (see also (Williams et al., 2013)). Our previous model was extended by comparing low-frequency and high-frequency OHCs, and extrapolating all calculations to body temperature (37ºC), including rat and gerbil to cover a wider frequency range. Most significantly, MET current amplitudes were corrected to 37ºC using a measured Q_{10} of 1.45 (Johnson et al., 2011) and the maximum PMCA2 pump rate was corrected using a Q_{10} of 2.8 (Carafoli, 1991; Schatzmann et al., 1969). For both cochlear locations, the independent variables were the Ca^{2+} load through the MET channels, and the number of PMCA2 pumps. The model differs from previous ones (Lumpkin et al., 1998; Ricci et al., 1998; Wu et al., 1996) in that both stereocilia and cell body were simulated simultaneously and the mitochondrial layer was added. The schematic of the model is illustrated (Fig. 5A), and the theoretical equations are given in the Appendix, along with the parameter values and their sources.

Ca^{2+} entering through the MET channels achieves its highest concentration at the tips of row 2 and row 3 stereocilia where the channels are located (Beurg et al., 2009). A gradient is established along the stereocilia and the concentration achieved at the top of the cell increases with load, reaching ~4 μM for the largest. The Ca^{2+} that has entered is transferred from the buffers to the pumps and mitochondria. With a small (7 pA) sustained load, Ca^{2+} is quickly absorbed by the calcium buffers (Fig. 5, yellow lines), which diffuse and are then freed over 10 to 20 sec by unbinding of the Ca^{2+} and extrusion by the PMCA2 pump (blue). With larger (14 pA) load, a small amount of Ca^{2+} is transiently buffered by the mitochondria (red). However, with the largest (21 pA) load, the mitochondria retain 20 percent of the Ca^{2+}, which is not pumped out over the time period simulated.

The Ca^{2+} kinetics in Fig. 5 were obtained with standard parameter values. The results of systematically changing the input (Ca^{2+} load, I_{Ca}, Fig. 6A) and output (PMCA2 number, Fig. 6B) on the cytosolic Ca^{2+} are shown in Fig. 6. The abscissae (X-axes) denote the ratio of the test condition (I_{Ca} or PMCA2 number) relative to the standard value. The Ca^{2+} at the soma rises as a result of both an increase in I_{Ca} or a decrease in PMCA2, but the high-frequency OHC is much more sensitive to variation than the low-frequency one. Thus, the somatic [Ca^{2+}] rises for smaller changes in I_{Ca} or PMCA2 density for basal OHCs than it does for apical low-frequency OHCs: variations in the parameters have little effect on the low-frequency OHC, but can cause substantial loading of the high-frequency OHC. The plots for basal and apical OHCs in both cases show about a ten-fold difference. This difference can be quantified by taking a [Ca^{2+}] of 0.5 μM (dashed lines in Fig. 6),

corresponding approximately to the threshold concentration at which the mitochondria start to accumulate Ca^{2+} (Xu et al., 1997), and comparing the equivalent abscissa values. For the PMCA2 density (Fig. 6B), the somatic Ca^{2+} of a basal OHC rises to 0.5 μM when the pump density is reduced to 0.65 of standard, but for an apical OHC, much greater reduction to 0.06 of standard is required cause the same Ca^{2+} elevation. The conclusion from these simulations is that high-frequency OHCs are much more vulnerable to variation in input or output factors. This accords with the effects of the *Tommy* and *Oblivion* PMCA2 mutations, in which pump rate is reduced, leading to hair cell death progressing from the basal high-frequency region. Furthermore, any reduction in mitochondrial health may cause diminished ATP production, thereby affecting the PMCA2 pumping efficiency. The results in Fig. 6 may also apply to loss of OHCs during excessive and prolonger noise stimulation; this amounts to an increase in load which will preferentially affect the high-frequency OHCs.

There are two main differences between hair cells in the low-frequency apical region compared to the high frequency basal region which underlie the greater likelihood of Ca^{2+} overload in high frequency OHCs. These are: (i) the larger amplitude of the MET current and a corresponding larger Ca^{2+} influx; and (ii) fewer PMCA2 pumps due to an approximately four-fold smaller bundle membrane area, which diminishes the Ca^{2+} extrusion rate. These two factors will exacerbate the vulnerability to ototoxic agents and overstimulation, but it seems likely that other differences may also contribute. For example, there has been the recent interesting observation that circadian clocks also vary along the tonotopic axis, with differences in timing being evident between low- and high-frequency regions of the mouse cochlea (Park et al., 2017). Noise exposure or other cochlear stresses may also result in opening of other Ca^{2+}- permeable ion channels, such as ATP-gated P2X receptors, which have been shown to mediate adaptation to high sound levels (Housley et al., 2013). Ca^{2+} influx via P2X2 channels may further increase the susceptibility of the high frequency OHCs. Exploring the origins and consequences of the cochlear gradients in cellular properties will continue to be a fruitful area of study in the peripheral auditory system.

Acknowledgements

The work was supported by grants RO1 DC1362 to RF and RO1 DC014685 to JHN from the National Institutes on Deafness and Other Communication Disorders.

APPENDIX

Description of model

Geometry:

Two hair cells were modeled and simulated, representing outer hair cells from the basal and apical turn of the gerbil cochlea, respectively. The heights of three stereociliary rows are 4.8, 4.0 and 3.2 μm for the apical hair cell and 1.2, 1.0 and 0.8 μm for the basal hair cell. Each stereocilium is 0.25 μm in dimeter, and the modeled cell body was 10 μm in depth. Considering the repeating pattern of the OHC stereociliary columns, the 3-D geometry was reduced to 2-D. That is, only one slice of the hair cell including a column of stereocilia, and the cell body below the column was simulated. The dimension of the simulated cell body

was 4.8×4.8×10 μm^3 (width×thickness×height). Considering this geometry, the diffusion in the stereocilia and cell body was computed in 1-D and 2-D, respectively. The diffusible space was divided into two sections along the depth (z-axis)—stereocilia ($z \geq 0$), and cell body ($z < 0$). A layer of mitochondria was at $-1 > z > -5$ μm. The mesh grid size was 0.1 μm in the stereocilia and between 0.2 and 1.0 μm in the cell body. The ratio of diffusible volumes was 0.8 and 0.6 in the stereocilia and soma.

Diffusion equation:

The dynamics of calcium consist of six components: 1) free calcium diffusion, binding kinetics with 2) fixed and 3) mobile buffers, 4) Ca^{2+} influx through the MT channels, 5) Ca^{2+} extrusion by PMCA pump combined by the leakage through the cell membrane and 6) Ca^{2+} update/return by the mitochondria. The overall governing equation is

$$\frac{dC}{dt} = D_{Ca}\nabla^2 C + \left(\frac{dC}{dt}\right)_{\text{Fix}} + \left(\frac{dC}{dt}\right)_{\text{Mob}} + \left(\frac{dC}{dt}\right)_{\text{Ext}} + \left(\frac{dC}{dt}\right)_{\text{Infl}} + \left(\frac{dC}{dt}\right)_{\text{Mito}}, \quad (1)$$

C is the free Ca^{2+} concentration and D_{Ca} is the Ca^{2+} diffusion coefficient (0.4 μm2/ms). The change of C due to a fixed buffer is

$$\left(\frac{dC}{dt}\right)_{\text{Fix}} = K_F^d k_F^+ \left(B_F^T - B_F\right) - k_F^+ C B_F, \quad (2)$$

where B_F^T and B_F are total and unbound concentration of the fixed buffer, K_F^d is the dissociation coefficient, and k_F^+ is finding rate of Ca^{2+} to the buffer. The change of C due to mobile buffers are governed by the first order kinetics and diffusion equation such as,

$$\left(\frac{dC}{dt}\right)_{\text{Mob}} = K_M^d k_M^+ \left(B_M^T - B_M\right) - k_M^+ C B_M, \text{ and} \quad (3)$$
$$\left(\frac{dB_M}{dt}\right)_{\text{Mob}} = \left(\frac{dC}{dt}\right)_{\text{Mob}} D_M \nabla^2 B_M,$$

where B_M^T and B_M are total and unbound concentration of the mobile buffer, K_M^d is the dissociation coefficient, and k_M^+ is binding rate of Ca^{2+} to the buffer.

Source and sink:

Ca^{2+} influx through the channel is defined according to Fick's first law.

$$\left(\frac{dC}{dt}\right)_{\text{Infl}} = -\frac{n_C i_{Ca}(t)}{2FV_C}, \quad (4)$$

where n_C is the number of transduction channel per stereocilia, i_{Ca} is the single channel calcium current, z is the valence of calcium ion, F is the Faraday constant, and V_C is the diffusible volume of the compartment. The calcium extrusion by PMCA pump was combined by the leakage through the cell membrane following (Sala et al., 1990).

$$\left(\frac{\partial C}{\partial t}\right)_{\text{Ext}} = \frac{v_{\max,PMCA} A_C}{V_C}\left(\frac{C_0}{C_0 + K_{PMCA}} + \frac{C}{C + K_{PMCA}}\right), \quad (5)$$

where $v_{max,PMCA}$ is the maximal velocity of transportation in mol/m^{2}s, A_C is the area of membrane of the compartment, K_{PMCA} is the half-maximal activation point of the PMCA pump and C_0 is the equilibrium point between the extrusion by PMCA pump and the leakage due to the Ca^{2+} gradient through membrane.

Mitochondria:

Based on anatomical evidence, it was assumed that the mitochondria lie in a belt, between 1 and 5 μm below the apical surface of the cell (−1> z ≥ −5 μm). This dimension of the mitochondrial belt was based on the following considerations. First, according to the observation of microscopic images (Beurg et al., 2010), the mitochondria density is highest just below the cuticular plate, and its volume fraction ranged between 0.2 and 0.6. Second, the mitochondrial Ca^{2+} transport is slower than other components of Ca^{2+} dynamics, such as the PMCA pump and buffering when the Ca^{2+} concentration is less than 0.5 μM (Xu et al., 1997). Finally, considering the steep Ca^{2+} gradient along the cell depth, the effect of fewer mitochondria below 5 μm from the cell top will be negligible. Therefore, adding mitochondria below this belt will have minimal effect on the simulated results (Ca^{2+} uptake by mitochondria due to excessive MET current). When Ca^{2+} through the stereocilia reaches the cytosol beneath the mitochondrial belt, more realistic mitochondrial and cell body model will be necessary. The rate of cytosolic free Ca^{2+} concentration change due to mitochondrial Ca^{2+} transport was composed of the flux into the mitochondria by the calcium uniporter ($J_{m,uni}$) and the flux out of the mitochondria by the sodium-calcium exchanger ($J_{m,NCX}$).

$$\left(\frac{dC}{dt}\right)_{Mito} = -J_{m,uni} + J_{m,NCX} \quad (6)$$

The rate of change of mitochondrial matrix free Ca^{2+} concentration (C_m) is

$$\frac{dC_m}{dt} = \frac{\kappa_m}{\gamma_m}\left(J_{m,uni} - J_{m,NCX}\right), \quad (7)$$

where κ_m is the ratio of free to fixed Ca^{2+} in the mitochondria and γ_m is the ratio of mitochondrial volume to diffusible cytosol volume. The kinetics of the mitochondria uniporter was reported to follow second order Hill equation (Gunter et al., 2000; Nicholls, 2005).

$$J_{mit,uni} = v_{\max,uni}\frac{C^2}{K_{uni}^2 + C^2}, \quad (8)$$

where $v_{max,uni}$ is the maximal calcium transportation rate of the uniporter in μM/ms, and K_{uni} is the half maximal activation point in μM. The v_{max} value of 114 μM/ms was derived from *in vitro* mitochondrial Ca^{2+} uptake rate of 4 nmol/min per 1 mg of mitochondria protein at $C = 0.5$ μM. For the K_{uni}, we chose 40 μM according to (Xu et al., 1997). Ca^{2+} extrusion from the mitochondria was governed by the first order relationship following Patterson et al. (2006).

$$J_{mit,NCX} = \frac{v_{\max,NCX}}{(1 + K_{NCX}/C_m)}, \quad (9)$$

where $v_{max,NCX}$ is the maximal rate of the sodium-calcium exchanger in μM/ms, and K_{NCX} is the half maximal activation point in μM. The parameter values are determined as follows. $\kappa_m = 2.5\times10^{-4}$ is from (Patterson et al., 2007). According to previous observation (Beurg et al., 2010), the ratio of mitochondria volume to total volume in the mitochondria belt is between 0.2 and 0.6. If we take the volume fraction of 0.4, $\gamma_m = 0.4/0.6 = 0.667$. The maximal extrusion rate $v_{max,NCX}$ of 1.81 μM/ms was chosen so that the mitochondria calcium transportation is balanced at $C = 0.5$ μM and $C_m = 0.05$ μM, and $K_{NCX} = 5$ μM (Patterson et al., 2007), similar to the plasma membrane NCX in cardiac muscle (Hilgemann et al., 1991). . The accuracy of model predication, at what Ca^{2+} influx level results in Ca^{2+} uptake by the mitochondria, depends on the C_m and K_{NCX} values.

Numerical solution:

Finite difference equations were derived by discretizing the partial differential equations then integrated using Crank-Nicholson method. The time step size was 10 μs. The computer code was written in Matlab (MathWorks, Natick, MA) and run on a PC (Intel i7–6700, 16 GB Ram). The code was validated by comparing the calcium influx rate calculated analytically with the summation of the change rate of free, buffered and extruded amount of calcium during simulation. This numerical error regarding mass conservation was about 0.2 percent which was used as a confidence-level of simulation. Initial conditions were as follows. The initial/resting calcium concentration was $C = 0.1$ μM, which is determined by the set point of the calcium pump-leakage equation, Eq. (5). Then the initial concentration of the buffers was obtained by static equilibrium with the 0.1 μM free Ca^{2+}. Because the Ca^{2+} equilibrium point of the mitochondria ($C = 0.5$ μM by Eq. (7) (Nicholls, 2005) is higher than that of the PMCA pump of cell membrane ($C = 0.1$ μM), at the channel closed initial state, the mitochondrial free calcium should be nearly depleted, and set to zero. Although these initial conditions are artificial, whether initial Ca^{2+}-level be at 0.1 or 0.5 μM has finite effect only a few ms after the onset.

References

Alharazneh A, Luk L, Huth M, Monfared A, Steyger PS, Cheng AG, Ricci AJ 2011 Functional hair cell mechanotransducer channels are required for aminoglycoside ototoxicity. PLoS One 6, e22347. [PubMed: 21818312]

Babcock DF, Herrington J, Goodwin PC, Park YB, Hille B 1997 Mitochondrial participation in the intracellular Ca2+ network. J. Cell Biol 136, 833–44. [PubMed: 9049249]

Baughman JM, Perocchi F, Girgis HS, Plovanich M, Belcher-Timme CA, Sancak Y, Bao XR, Strittmatter L, Goldberger O, Bogorad RL, Koteliansky V, Mootha VK 2011 Integrative genomics identifies MCU as an essential component of the mitochondrial calcium uniporter. Nature 476, 341–5. [PubMed: 21685886]

Bernardi P, Di Lisa F 2015 The mitochondrial permeability transition pore: molecular nature and role as a target in cardioprotection. J. Mol. Cell. Cardiol 78, 100–6. [PubMed: 25268651]

Beurg M, Evans MG, Hackney CM, Fettiplace R 2006 A large-conductance calcium- selective mechanotransducer channel in mammalian cochlear hair cells. J. Neurosci 26, 10992–1000. [PubMed: 17065441]

Beurg M, Fettiplace R, Nam JH, Ricci AJ 2009 Localization of inner hair cell mechanotransducer channels using high-speed calcium imaging. Nat. Neurosci 12, 553–8. [PubMed: 19330002]

Beurg M, Nam JH, Chen Q, Fettiplace R 2010 Calcium balance and mechanotransduction in rat cochlear hair cells. J. Neurophysiol 104, 18–34. [PubMed: 20427623]

Bork JM, Peters LM, Riazuddin S, Bernstein SL, Ahmed ZM, Ness SL, Polomeno R, Ramesh A, Schloss M, Srisailpathy CR, Wayne S, Bellman S, Desmukh D, Ahmed Z, Khan SN, Kaloustian VM, Li XC, Lalwani A, Riazuddin S, Bitner-Glindzicz M, Nance WE, Liu XZ, Wistow G, Smith RJ, Griffith AJ, Wilcox ER, Friedman TB, Morell RJ 2001 Usher syndrome 1D and nonsyndromic autosomal recessive deafness DFNB12 are caused by allelic mutations of the novel cadherin-like gene CDH23. Am. J. Hum. Genet 68, 26–37. [PubMed: 11090341]

Bortolozzi M, Mammano F 2018 PMCA2 pump mutations and hereditary deafness. Neurosci. Lett 663, 18–24. [PubMed: 29452611]

Bortolozzi M, Brini M, Parkinson N, Crispino G, Scimemi P, De Siati RD, Di Leva F, Parker A, Ortolano S, Arslan E, Brown SD, Carafoli E, Mammano F 2010 The novel PMCA2 pump mutation Tommy impairs cytosolic calcium clearance in hair cells and links to deafness in mice. J. Biol. Chem 285, 37693–703. [PubMed: 20826782]

Bosher SK, Warren RL 1978 Very low calcium content of cochlear endolymph, an extracellular fluid. Nature 273, 377–8. [PubMed: 661948]

Brandt A, Striessnig J, Moser T 2003 CaV1.3 channels are essential for development and presynaptic activity of cochlear inner hair cells. J. Neurosci 23, 10832–40. [PubMed: 14645476]

Brini M 2003 Ca(2+) signalling in mitochondria: mechanism and role in physiology and pathology. Cell Calcium 34, 399–405. [PubMed: 12909084]

Brock PR, Maibach R, Childs M, Rajput K, Roebuck D, Sullivan MJ, Laithier V, Ronghe M, Dall'Igna P, Hiyama E, Brichard B, Skeen J, Mateos ME, Capra M, Rangaswami AA, Ansari M, Rechnitzer C, Veal GJ, Covezzoli A, Brugieres L, Perilongo G, Czauderna P, Morland B, Neuwelt EA 2018 Sodium Thiosulfate for Protection from Cisplatin-Induced Hearing Loss. N. Engl. J. Med 378, 2376–2385. [PubMed: 29924955]

Carafoli E 1991 Calcium pump of the plasma membrane. Physiol. Rev 71, 129–53. [PubMed: 1986387]

Carafoli E, Stauffer T 1994 The plasma membrane calcium pump: functional domains, regulation of the activity, and tissue specificity of isoform expression. J. Neurobiol 25, 312–24. [PubMed: 8195792]

Chen Q, Mahendrasingam S, Tickle JA, Hackney CM, Furness DN, Fettiplace R 2012 The development, distribution and density of the plasma membrane calcium ATPase 2 calcium pump in rat cochlear hair cells. Eur. J. Neurosci 36, 2302–10. [PubMed: 22672315]

Corns LF, Johnson SL, Kros CJ, Marcotti W 2014 Calcium entry into stereocilia drives adaptation of the mechanoelectrical transducer current of mammalian cochlear hair cells. Proc. Natl. Acad. Sci. U. S. A 111, 14918–23. [PubMed: 25228765]

Cortopassi G, Hutchin T 1994 A molecular and cellular hypothesis for aminoglycoside-nduced deafness. Hear. Res 78, 27–30. [PubMed: 7961174]

Cruickshanks KJ, Wiley TL, Tweed TS, Klein BE, Klein R, Mares-Perlman JA, Nondahl DM 1998 Prevalence of hearing loss in older adults in Beaver Dam, Wisconsin. The Epidemiology of Hearing Loss Study. Am. J. Epidemiol 148, 879–86. [PubMed: 9801018]

Dallos P, Harris D 1978 Properties of auditory nerve responses in absence of outer hair cells. . Neurophysiol 41, 365–83.

Dallos P, Wu X, Cheatham MA, Gao J, Zheng J, Anderson CT, Jia S, Wang X, Cheng WH, Sengupta S, He DZ, Zuo J 2008 Prestin-based outer hair cell motility is necessary for mammalian cochlear amplification. Neuron 58, 333–9. [PubMed: 18466744]

David G, Barrett JN, Barrett EF 1998 Evidence that mitochondria buffer physiological Ca2+ loads in lizard motor nerve terminals. J. Physiol 509 (Pt 1), 59–65. [PubMed: 9547381]

De Stefani D, Rizzuto R, Pozzan T 2016 Enjoy the Trip: Calcium in Mitochondria Back and Forth. Annu. Rev. Biochem 85, 161–92. [PubMed: 27145841]

De Stefani D, Raffaello A, Teardo E, Szabo I, Rizzuto R 2011 A forty-kilodalton protein of the inner membrane is the mitochondrial calcium uniporter. Nature 476, 336–40. [PubMed: 21685888]

Dror AA, Avraham KB 2010 Hearing impairment: a panoply of genes and functions. Neuron 68, 293–308. [PubMed: 20955936]

Dumont RA, Lins U, Filoteo AG, Penniston JT, Kachar B, Gillespie PG 2001 Plasma membrane Ca2+-ATPase isoform 2a is the PMCA of hair bundles. J. Neurosci 21, 5066–78. [PubMed: 11438582]

Esterberg R, Linbo T, Pickett SB, Wu P, Ou HC, Rubel EW, Raible DW 2016 Mitochondrial calcium uptake underlies ROS generation during aminoglycoside-induced hair cell death. J. Clin. Invest 126, 3556–66. [PubMed: 27500493]

Fettiplace R 2016 Is TMC1 the Hair Cell Mechanotransducer Channel? Biophys. J 111, 3–9. [PubMed: 27410728]

Fettiplace R 2017 Hair Cell Transduction, Tuning, and Synaptic Transmission in the Mammalian Cochlea. Compr Physiol 7, 1197–1227. [PubMed: 28915323]

Ficarella R, Di Leva F, Bortolozzi M, Ortolano S, Donaudy F, Petrillo M, Melchionda S, Lelli A, Domi T, Fedrizzi L, Lim D, Shull GE, Gasparini P, Brini M, Mammano F, Carafoli E 2007 A functional study of plasma-membrane calcium-pump isoform 2 mutants causing digenic deafness. Proc. Natl. Acad. Sci. U. S. A 104, 1516–21. [PubMed: 17234811]

Gates GA, Couropmitree NN, Myers RH 1999 Genetic associations in age-related hearing thresholds. Arch. Otolaryngol. Head Neck Surg 125, 654–9. [PubMed: 10367922]

Gill SS, Salt AN 1997 Quantitative differences in endolymphatic calcium and endocochlear potential between pigmented and albino guinea pigs. Hear. Res 113, 191–7. [PubMed: 9387998]

Gomez-Casati ME, Fuchs PA, Elgoyhen AB, Katz E 2005 Biophysical and pharmacological characterization of nicotinic cholinergic receptors in rat cochlear inner hair cells. J. Physiol 566, 103–18. [PubMed: 15860528]

Gunter TE, Buntinas L, Sparagna G, Eliseev R, Gunter K 2000 Mitochondrial calcium transport: mechanisms and functions. Cell Calcium 28, 285–96. [PubMed: 11115368]

Hackney CM, Mahendrasingam S, Jones EM, Fettiplace R 2003 The distribution of calcium buffering proteins in the turtle cochlea. J. Neurosci 23, 4577–89. [PubMed: 12805298]

Hackney CM, Mahendrasingam S, Penn A, Fettiplace R 2005 The concentrations of calcium buffering proteins in mammalian cochlear hair cells. J. Neurosci 25, 7867–75. [PubMed: 16120789]

Heizmann CW, Berchtold MW, Rowlerson AM 1982 Correlation of parvalbumin concentration with relaxation speed in mammalian muscles. Proc. Natl. Acad. Sci. U. S. A 79, 7243–7. [PubMed: 6961404]

Hilgemann DW, Collins A, Cash DP, Nagel GA 1991 Cardiac Na(+)-Ca2+ exchange system in giant membrane patches. Ann. N. Y. Acad. Sci 639, 126–39. [PubMed: 1785836]

Hilgert N, Smith RJ, Van Camp G 2009 Forty-six genes causing nonsyndromic hearing impairment: which ones should be analyzed in DNA diagnostics? Mutat. Res 681, 189–96. [PubMed: 18804553]

Hill JK, Williams DE, LeMasurier M, Dumont RA, Strehler EE, Gillespie PG 2006 Splice-site A choice targets plasma-membrane Ca2+-ATPase isoform 2 to hair bundles. J. Neurosci 26, 6172–80. [PubMed: 16763025]

Hodgkin AL, McNaughton PA, Nunn BJ 1987 Measurement of sodium-calcium exchange in salamander rods. J. Physiol 391, 347–70. [PubMed: 2451008]

Housley GD, Morton-Jones R, Vlajkovic SM, Telang RS, Paramananthasivam V, Tadros SF, Wong AC, Froud KE, Cederholm JM, Sivakumaran Y, Snguanwongchai P, Khakh BS, Cockayne DA, Thorne PR, Ryan AF 2013 ATP- gated ion channels mediate adaptation to elevated sound levels. Proc. Natl. Acad. Sci. U. S. A 110, 7494–9. [PubMed: 23592720]

Ikeda K, Kusakari J, Takasaka T, Saito Y 1987 The Ca2+ activity of cochlear endolymph of the guinea pig and the effect of inhibitors. Hear. Res 26, 117–25. [PubMed: 3644819]

Imamura S, Adams JC 1996 Immunolocalization of peptide 19 and other calcium-binding proteins in the guinea pig cochlea. Anat. Embryol. (Berl.) 194, 407–18. [PubMed: 8896705]

Jaiganesh A, De-la-Torre P, Patel AA, Termine DJ, Velez-Cortes F, Chen C, Sotomayor M 2018 Zooming in on Cadherin-23: Structural Diversity and Potential Mechanisms of Inherited Deafness. Structure

Jayakody DMP, Friedland PL, Martins RN, Sohrabi HR 2018 Impact of Aging on the Auditory System and Related Cognitive Functions: A Narrative Review. Front. Neurosci 12, 125. [PubMed: 29556173]

Johnson SL, Beurg M, Marcotti W, Fettiplace R 2011 Prestin-driven cochlear amplification is not limited by the outer hair cell membrane time constant. Neuron 70, 1143–54. [PubMed: 21689600]

Johnson SL, Kennedy HJ, Holley MC, Fettiplace R, Marcotti W 2012 The resting transducer current drives spontaneous activity in prehearing mammalian cochlear inner hair cells. J. Neurosci 32, 10479–83. [PubMed: 22855797]

Kamogashira T, Fujimoto C, Yamasoba T 2015 Reactive oxygen species, apoptosis, and mitochondrial dysfunction in hearing loss. Biomed Res Int 2015, 617207. [PubMed: 25874222]

Kawashima Y, Geleoc GS, Kurima K, Labay V, Lelli A, Asai Y, Makishima T, Wu DK, Della Santina CC, Holt JR, Griffith AJ 2011 Mechanotransduction in mouse inner ear hair cells requires transmembrane channel-like genes. J. Clin. Invest 121, 4796–809. [PubMed: 22105175]

Kiang NY, Liberman MC, Sewell WF, Guinan JJ 1986 Single unit clues to cochlear mechanisms. Hear. Res 22, 171–82. [PubMed: 3733538]

Knirsch M, Brandt N, Braig C, Kuhn S, Hirt B, Munkner S, Knipper M, Engel J 2007 Persistence of Ca(v)1.3 Ca2+ channels in mature outer hair cells supports outer hair cell afferent signaling. J. Neurosci 27, 6442–51. [PubMed: 17567805]

Kozel PJ, Friedman RA, Erway LC, Yamoah EN, Liu LH, Riddle T, Duffy JJ, Doetschman T, Miller ML, Cardell EL, Shull GE 1998 Balance and hearing deficits in mice with a null mutation in the gene encoding plasma membrane Ca2+- ATPase isoform 2. J. Biol. Chem 273, 18693–6. [PubMed: 9668038]

Kurima K, Peters LM, Yang Y, Riazuddin S, Ahmed ZM, Naz S, Arnaud D, Drury S, Mo J, Makishima T, Ghosh M, Menon PS, Deshmukh D, Oddoux C, Ostrer H, Khan S, Riazuddin S, Deininger PL, Hampton LL, Sullivan SL, Battey JF Jr., Keats BJ, Wilcox ER, Friedman TB, Griffith AJ 2002 Dominant and recessive deafness caused by mutations of a novel gene, TMC1, required for cochlear hair-cell function. Nat. Genet 30, 277–84. [PubMed: 11850618]

Lee SH, Schwaller B, Neher E 2000 Kinetics of Ca2+ binding to parvalbumin in bovine chromaffin cells: implications for [Ca2+] transients of neuronal dendrites. J. Physiol 525 Pt 2, 419–32. [PubMed: 10835044]

Liang Y, Wang A, Belyantseva IA, Anderson DW, Probst FJ, Barber TD, Miller W, Touchman JW, Jin L, Sullivan SL, Sellers JR, Camper SA, Lloyd RV, Kachar B, Friedman TB, Fridell RA 1999 Characterization of the human and mouse unconventional myosin XV genes responsible for hereditary deafness DFNB3 and shaker 2. Genomics 61, 243–58. [PubMed: 10552926]

Liberman MC 2016 Noise-Induced Hearing Loss: Permanent Versus Temporary Threshold Shifts and the Effects of Hair Cell Versus Neuronal Degeneration. Adv. Exp. Med. Biol 875, 1–7. [PubMed: 26610938]

Liberman MC, Kiang NY 1978 Acoustic trauma in cats. Cochlear pathology and auditory-nerve activity. Acta Otolaryngol. Suppl 358, 1–63. [PubMed: 281107]

Lim DJ 1986 Functional structure of the organ of Corti: a review. Hear. Res 22, 117–46. [PubMed: 3525482]

Lumpkin EA, Hudspeth AJ 1998 Regulation of free Ca2+ concentration in hair-cell stereocilia. J. Neurosci 18, 6300–18. [PubMed: 9698322]

Luo DG, Xue T, Yau KW 2008 How vision begins: an odyssey. Proc. Natl. Acad. Sci. U. S. A 105, 9855–62. [PubMed: 18632568]

Mammano F 2011 Ca^{2+} homeostasis defects and hereditary hearing loss. Biofactors 37, 182–8. [PubMed: 21698697]

McCullough BJ, Tempel BL 2004 Haplo-insufficiency revealed in deafwaddler mice when tested for hearing loss and ataxia. Hear. Res 195, 90–102. [PubMed: 15350283]

Michalak M, Groenendyk J, Szabo E, Gold LI, Opas M 2009 Calreticulin, a multi-process calcium-buffering chaperone of the endoplasmic reticulum. Biochem. J 417, 651–66. [PubMed: 19133842]

Michalski N, Petit C 2015 Genetics of auditory mechano-electrical transduction. Pflugers Arch 467, 49–72. [PubMed: 24957570]

Morciano G, Giorgi C, Bonora M, Punzetti S, Pavasini R, Wieckowski MR, Campo G, Pinton P 2015 Molecular identity of the mitochondrial permeability transition pore and its role in ischemia-reperfusion injury. J. Mol. Cell. Cardiol 78, 142–53. [PubMed: 25172387]

Nagerl UV, Novo D, Mody I, Vergara JL 2000 Binding kinetics of calbindin-D(28k) determined by flash photolysis of caged Ca(2+). Biophys. J 79, 3009–18. [PubMed: 11106608]

Nakazawa K 2001 Ultrastructural localization of calmodulin in gerbil cochlea by immunogold electron microscopy. Hear. Res 151, 133–140. [PubMed: 11124460]

Nicholls DG 2005 Mitochondria and calcium signaling. Cell Calcium 38, 311–7. [PubMed: 16087232]

Noben-Trauth K, Zheng QY, Johnson KR 2003 Association of cadherin 23 with polygenic inheritance and genetic modification of sensorineural hearing loss. Nat. Genet 35, 21–3.

Ohmori H 1985 Mechano-electrical transduction currents in isolated vestibular hair cells of the chick. J. Physiol 359, 189–217. [PubMed: 2582113]

Pack AK, Slepecky NB 1995 Cytoskeletal and calcium-binding proteins in the mammalian organ of Corti: cell type-specific proteins displaying longitudinal and radial gradients. Hear. Res 91, 119–35. [PubMed: 8647714]

Park JS, Cederroth CR, Basinou V, Sweetapple L, Buijink R, Lundkvist GB, Michel S, Canlon B 2017 Differential Phase Arrangement of Cellular Clocks along the Tonotopic Axis of the Mouse Cochlea Ex Vivo. Curr. Biol 27, 2623–2629.e2. [PubMed: 28823676]

Patterson M, Sneyd J, Friel DD 2007 Depolarization-induced calcium responses in sympathetic neurons: relative contributions from Ca2+ entry, extrusion, ER/mitochondrial Ca2+ uptake and release, and Ca2+ buffering. J. Gen. Physiol 129, 29–56. [PubMed: 17190902]

Ricci AJ, Wu YC, Fettiplace R 1998 The endogenous calcium buffer and the time course of transducer adaptation in auditory hair cells. J. Neurosci 18, 8261–77. [PubMed: 9763471]

Rizzuto R, De Stefani D, Raffaello A, Mammucari C 2012 Mitochondria as sensors and regulators of calcium signalling. Nat. Rev. Mol. Cell Biol 13, 566–78. [PubMed: 22850819]

Roth B, Bruns V 1992 Postnatal development of the rat organ of Corti. II. Hair cell receptors and their supporting elements. Anat. Embryol. (Berl.) 185, 571–81. [PubMed: 1605368]

Ryan AF, Woolf NK, Bone RC 1980 Ultrastructural correlates of selective outer hair cell destruction following kanamycin intoxication in the chinchilla. Hear. Res 3, 335–51. [PubMed: 7451380]

Sabatini BL, Oertner TG, Svoboda K 2002 The life cycle of Ca(2+) ions in dendritic spines. Neuron 33, 439–52. [PubMed: 11832230]

Sakaguchi N, Henzl MT, Thalmann I, Thalmann R, Schulte BA 1998 Oncomodulin is expressed exclusively by outer hair cells in the organ of Corti. J. Histochem. Cytochem 46, 29–40. [PubMed: 9405492]

Sala F, Hernandez-Cruz A 1990 Calcium diffusion modeling in a spherical neuron. Relevance of buffering properties. Biophys. J 57, 313–24. [PubMed: 2317553]

Salt AN, Inamura N, Thalmann R, Vora A 1989 Calcium gradients in inner ear endolymph. Am. J. Otolaryngol 10, 371–5. [PubMed: 2596623]

Schatzmann HJ, Vincenzi FF 1969 Calcium movements across the membrane of human red cells. J. Physiol 201, 369–95. [PubMed: 4238381]

Schmidt H, Brown EB, Schwaller B, Eilers J 2003 Diffusional mobility of parvalbumin in spiny dendrites of cerebellar Purkinje neurons quantified by fluorescence recovery after photobleaching. Biophys. J 84, 2599–608. [PubMed: 12668468]

Schultz JM, Yang Y, Caride AJ, Filoteo AG, Penheiter AR, Lagziel A, Morell RJ, Mohiddin SA, Fananapazir L, Madeo AC, Penniston JT, Griffith AJ 2005 Modification of human hearing loss by plasma-membrane calcium pump PMCA2. N. Engl. J. Med 352, 1557–64. [PubMed: 15829536]

Schwaller B 2010 Cytosolic Ca2+ buffers. Cold Spring Harb. Perspect. Biol 2, a004051.

Schwaller B, Dick J, Dhoot G, Carroll S, Vrbova G, Nicotera P, Pette D, Wyss A, Bluethmann H, Hunziker W, Celio MR 1999 Prolonged contraction-relaxation cycle of fast-twitch muscles in parvalbumin knockout mice. Am. J. Physiol 276, C395–403. [PubMed: 9950767]

Sheth S, Mukherjea D, Rybak LP, Ramkumar V 2017 Mechanisms of Cisplatin-Induced Ototoxicity and Otoprotection. Front. Cell. Neurosci 11, 338. [PubMed: 29163050]

Spiden SL, Bortolozzi M, Di Leva F, de Angelis MH, Fuchs H, Lim D, Ortolano S, Ingham NJ, Brini M, Carafoli E, Mammano F, Steel KP 2008 The novel mouse mutation Oblivion inactivates the PMCA2 pump and causes progressive hearing loss. PLoS Genet 4, e1000238. [PubMed: 18974863]

Street VA, McKee-Johnson JW, Fonseca RC, Tempel BL, Noben-Trauth K 1998 Mutations in a plasma membrane Ca2+-ATPase gene cause deafness in deafwaddler mice. Nat. Genet 19, 390–4. [PubMed: 9697703]

Tong B, Hornak AJ, Maison SF, Ohlemiller KK, Liberman MC, Simmons DD 2016 Oncomodulin, an EF-Hand Ca2+ Buffer, Is Critical for Maintaining Cochlear Function in Mice. J. Neurosci 36, 1631–5. [PubMed: 26843644]

Tucker T, Fettiplace R 1995 Confocal imaging of calcium microdomains and calcium extrusion in turtle hair cells. Neuron 15, 1323–35. [PubMed: 8845156]

Vona B, Nanda I, Hofrichter MA, Shehata-Dieler W, Haaf T 2015 Non-syndromic hearing loss gene identification: A brief history and glimpse into the future. Mol. Cell. Probes 29, 260–70. [PubMed: 25845345]

Vreugde S, Erven A, Kros CJ, Marcotti W, Fuchs H, Kurima K, Wilcox ER, Friedman TB, Griffith AJ, Balling R, Hrabe De Angelis M, Avraham KB, Steel KP 2002 Beethoven, a mouse model for dominant, progressive hearing loss DFNA36. Nat. Genet 30, 257–8. [PubMed: 11850623]

Watson CJ, Tempel BL 2013 A new Atp2b2 deafwaddler allele, dfw(i5), interacts strongly with Cdh23 and other auditory modifiers. Hear. Res 304, 41–8. [PubMed: 23792079]

Weisz CJ, Lehar M, Hiel H, Glowatzki E, Fuchs PA 2012 Synaptic transfer from outer hair cells to type II afferent fibers in the rat cochlea. J. Neurosci 32, 9528–36. [PubMed: 22787038]

Williams GS, Boyman L, Chikando AC, Khairallah RJ, Lederer WJ 2013 Mitochondrial calcium uptake. Proc. Natl. Acad. Sci. U. S. A 110, 10479–86. [PubMed: 23759742]

Wingrove DE, Amatruda JM, Gunter TE 1984 Glucagon effects on the membrane potential and calcium uptake rate of rat liver mitochondria. J. Biol. Chem 259, 9390–4. [PubMed: 6204980]

Wood JD, Muchinsky SJ, Filoteo AG, Penniston JT, Tempel BL 2004 Low endolymph calcium concentrations in deafwaddler2J mice suggest that PMCA2 contributes to endolymph calcium maintenance. Journal of the Association for Research in Otolaryngology : JARO 5, 99–110. [PubMed: 15357414]

Wu YC, Tucker T, Fettiplace R 1996 A theoretical study of calcium microdomains in turtle hair cells. Biophys. J 71, 2256–75. [PubMed: 8913569]

Xu T, Naraghi M, Kang H, Neher E 1997 Kinetic studies of Ca2+ binding and Ca2+ clearance in the cytosol of adrenal chromaffin cells. Biophys. J 73, 532–45. [PubMed: 9199815]

Yamoah EN, Lumpkin EA, Dumont RA, Smith PJ, Hudspeth AJ, Gillespie PG 1998 Plasma membrane Ca2+-ATPase extrudes Ca2+ from hair cell stereocilia. J. Neurosci 18, 610–24. [PubMed: 9425003]

Yau KW, Nakatani K 1984 Electrogenic Na-Ca exchange in retinal rod outer segment. Nature 311, 661–3. [PubMed: 6434995]

Yuste R, Majewska A, Holthoff K 2000 From form to function: calcium compartmentalization in dendritic spines. Nat. Neurosci 3, 653–9. [PubMed: 10862697]

Zheng J, Shen W, He DZ, Long KB, Madison LD, Dallos P 2000 Prestin is the motor protein of cochlear outer hair cells. Nature 405, 149–55. [PubMed: 10821263]

Zhou Z, Neher E 1993 Mobile and immobile calcium buffers in bovine adrenal chromaffin cells. J. Physiol 469, 245–73. [PubMed: 8271200]

Zorov DB, Juhaszova M, Sollott SJ 2014 Mitochondrial reactive oxygen species (ROS) and ROS-induced ROS release. Physiol. Rev 94, 909–50. [PubMed: 24987008]

Highlights

Environmental hearing deficits correlated with loss of basal outer hair cells (OHCs) Vulnerability reflects differences in Ca^{2+} balance among cochlear hair cells. Calcium homeostasis modeled using available experimental parameters OHCs have two distinct micro-compartments, hair bundle and soma, for Ca^{2+} handling Basal OHCs most susceptible due to larger transducer currents and smaller size

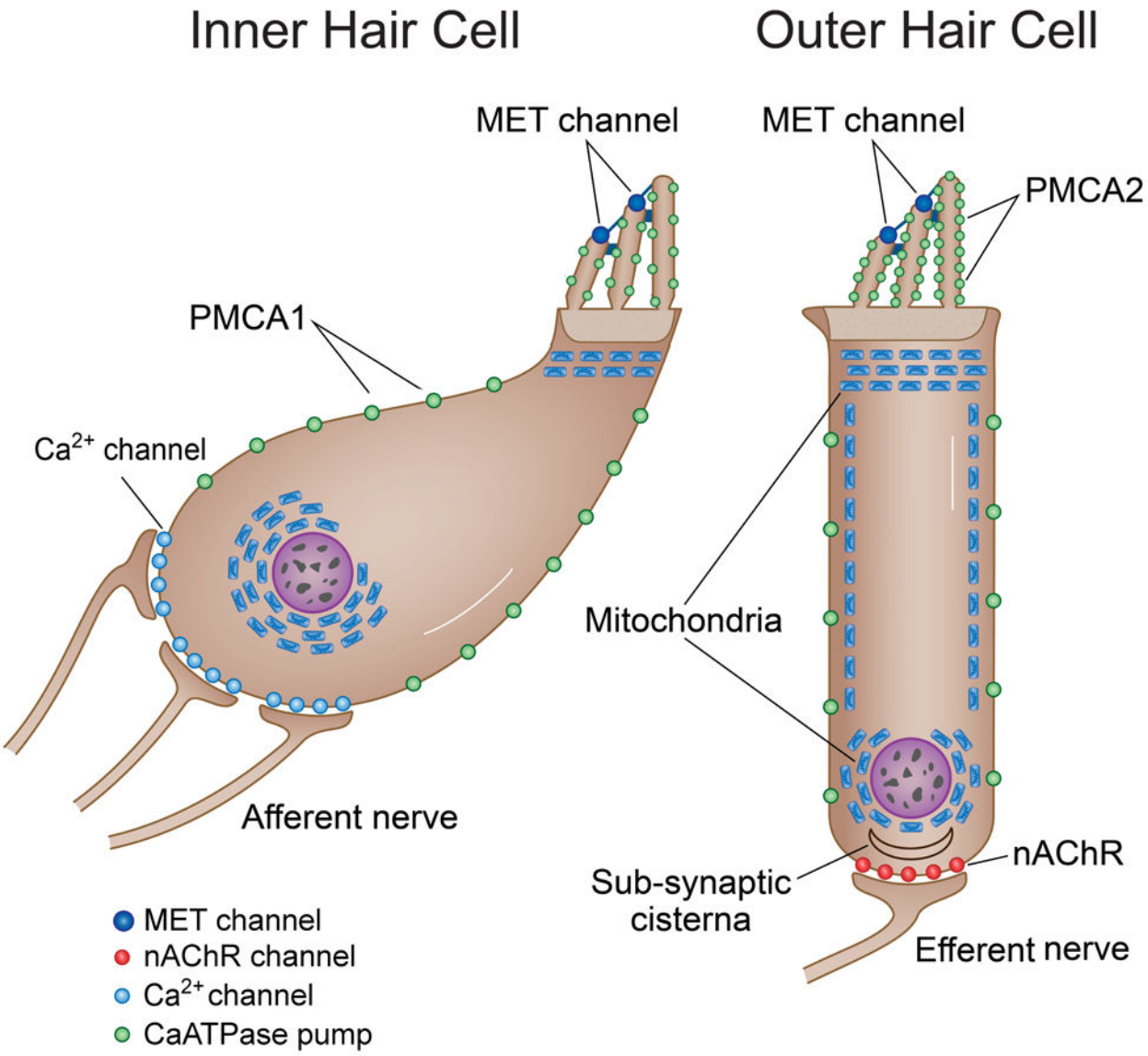

Fig. 1.

Factors involved in Ca^{2+} homeostasis in cochlear inner hair cells (IHCs) and outer hair cells (OHCs). Ca^{2+} enters via mechanotransducer (MET) channels in the stereocilia of both hair cell types, and also via voltage-dependent Ca^{2+} channels (mainly IHCs) and nicotinic acetylcholine receptors (nAChR) in OHCs. Ca^{2+} is buffered by cytoplasmic calcium binding proteins and by fixed organelles, mitochondria and sub-synaptic cisternae. Ca^{2+} is extruded by a plasma membrane CaATPase pump, PMCA2 in the OHC and IHC stereocilia, and PMCA1 in the IHC soma.

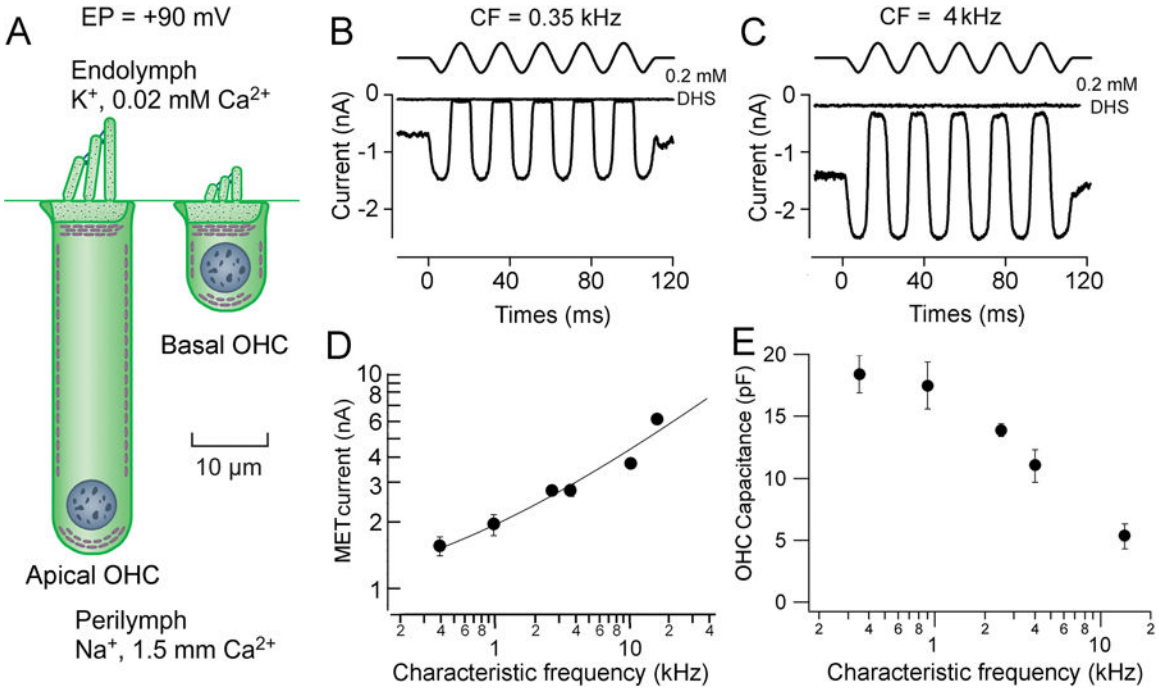

Fig. 2.

Variation in OHC properties with cochlear location. A. Basal high-frequency hair cells are about a third the dimensions but have four times the amplitude of MET current, and hence Ca^{2+} load. The route of Ca^{2+} entry in OHCs is principally via MET channels in the hair bundle bathed in endolymph with a low Ca^{2+} concentration of 20 µM. B, C. Recordings of MET currents in response to maximal bundle vibrations are shown for two cochlear locations, holding potential −84 mV. Note that for both low-frequency (0.35 kHz) and mid-frequency (4 kHz) OHCs, about half the maximum MET current is activated at rest, and will be constantly flowing into the cell as a 'silent current'. Application of 0.2 mM dihydrostreptomycin (DHS) defines the zero, non-MET current, level. D. The MET current amplitude increases with characteristic frequency (CF); current amplitudes have been corrected to body temperature 37ºC using a measured Q_{10} of 1.45 (Johnson et al., 2011). Results are from cochleas of gerbil (two lowest CFs; postnatal day (P)6 – P28), and rat (P8 – P19). E. The size of the cells, indicated by their electrical capacitance, decreases with frequency. Data from (Johnson et al., 2011)

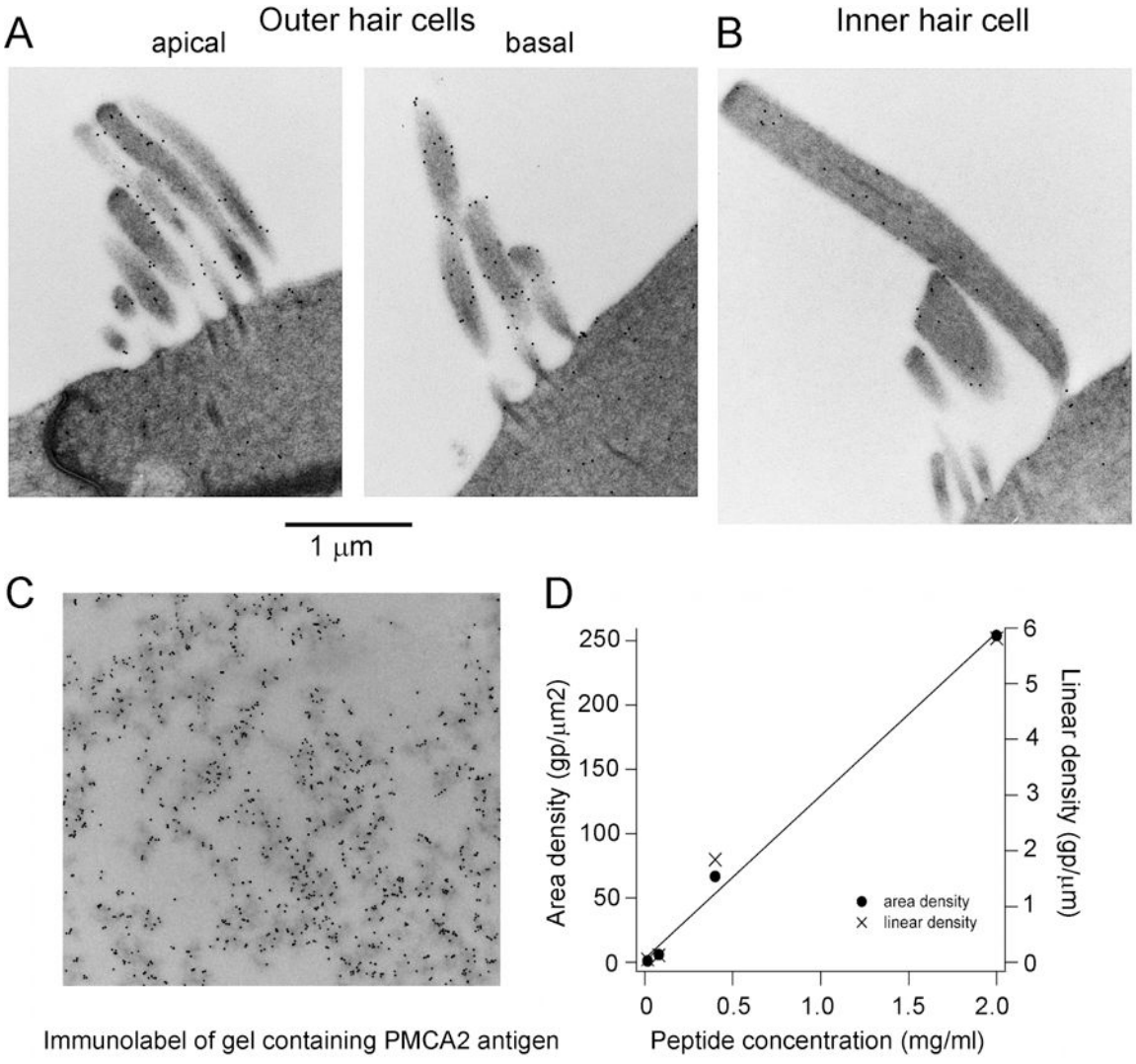

Fig. 3.

Immunogold quantification of the PMCA2 plasma membrane CaATPase pump. A, B Labeling of stereociliary bundles of apical and basal OHCs is greater than that of an IHC. C. Immunogold labeling of a section of gel impregnated with the PMCA2 peptide antigen. D. Immunogold counts for four different concentrations of antigen, measurements taken for the total area or for intersection of a line drawn across the section. The calibration was used to determine the pump density in hair cell stereocilia. Modified from (Chen et al., 2012).

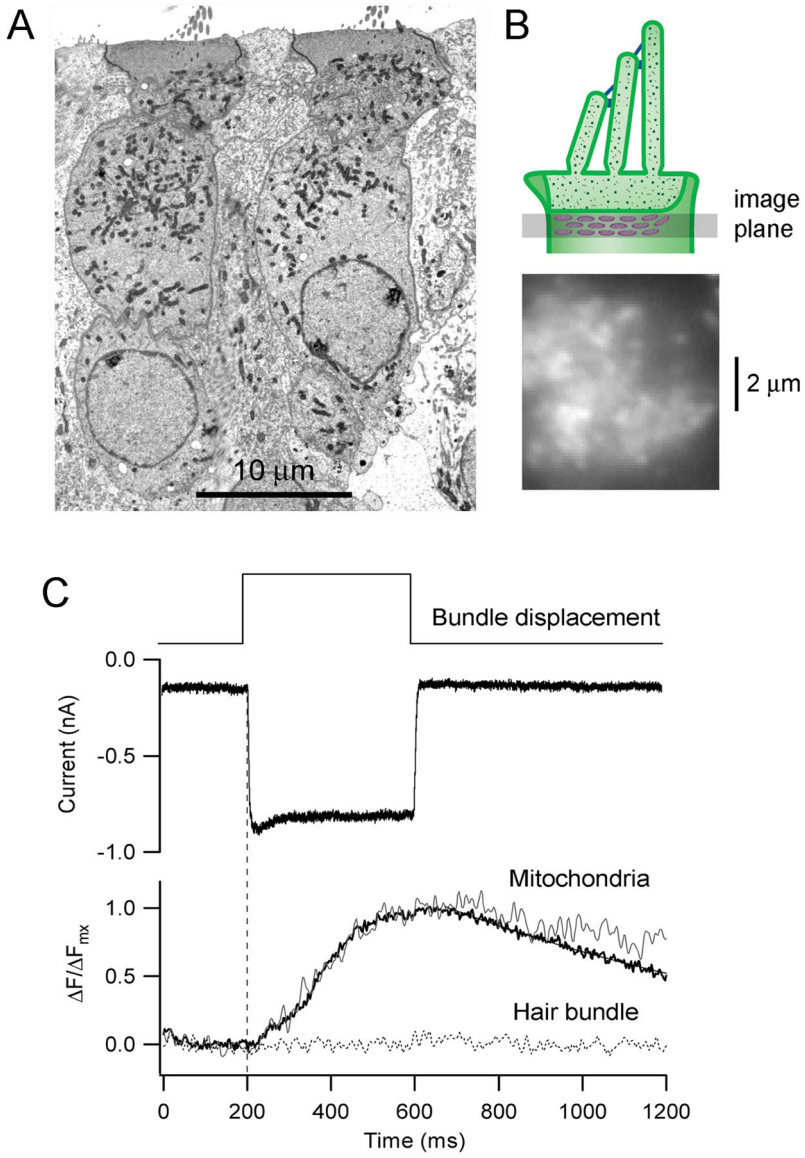

Fig. 4.

Ca^{2+} uptake into the sub-cuticular plate mitochondria. A. Transmission electron micrograph of two OHCs in a P10 rat organ of Corti, showing the high density of mitochondria in the supranuclear region of cytoplasm. B. Top depicts the imaging plane for measuring the Ca^{2+} fluorescence in mitochondria filled with calcium dye Rhod2; below shows a top view of the OHC with the bright regions being mitochondrial densities. C. MET current (holding potential of −84 mV) and mitochondrial Ca^{2+} fluorescence in an OHC in response to hair bundle deflection. The mitochondrial fluorescence, expressed as $\Delta F/\Delta F_{max}$, illustrates a single cell (noisy trace) and an average of five different cells (bold trace), showing that Ca^{2+} accumulates during the bundle stimulus. The dotted line represents imaging of the hair bundle, where no signal was detected. Results taken from (Beurg et al., 2010).

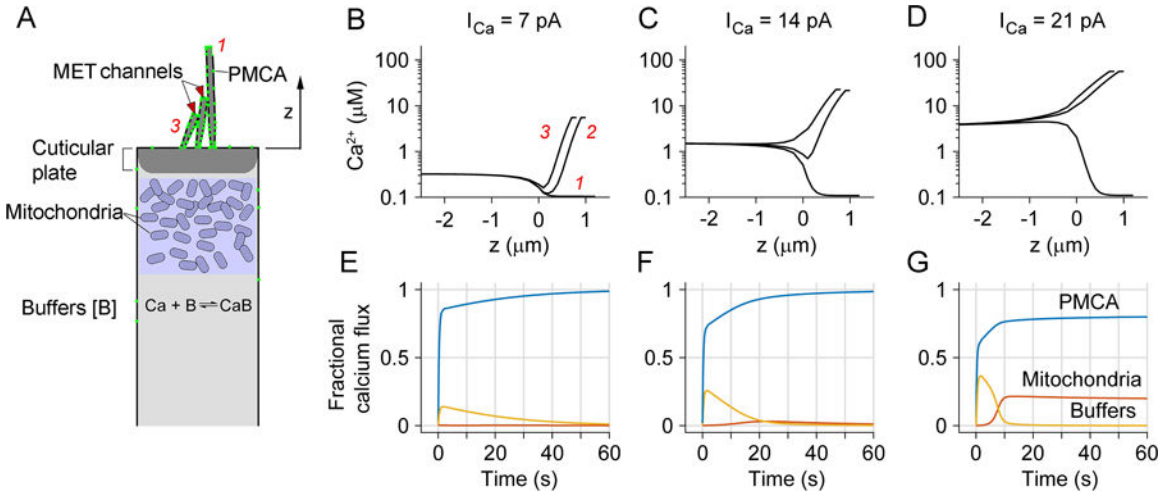

Fig. 5.

Modeling Ca^{2+} homeostasis in an OHC. A. Schematic hair cell showing components of the model, including Ca^{2+} influx through MET channels at tips of second and third row stereocilia, buffering by mitochondria and cytoplasmic Ca^{2+} binding proteins, and extrusion via PMCA in stereocilia. The height of the tallest stereocilium above top of cell is z = 4 μm for an apical OHC and 1 μm for a basal OHC; the number of OHC tip links is 54 (apex) and 72 (base). B, C, D. Simulations of Ca^{2+} changes during sustained loads of 7 pA, 14 pA and 21 pA flowing in through the MET channels in the bundle of a basal OHC. In each plot, the time course of cytoplasmic [Ca^{2+}] is shown as a function of distance from the top of the cell, z = 0, for the three rows of stereocilia, indicated in B as red numbers, *1*, *2* and *3* for first, second and third row. Negative values of z denote distances below top of cell. These are the steady-state concentrations at the end of the 60 s stimulus. Note that for larger loads, [Ca^{2+}] at the top of the cell is 1.5 to 4 μM. E, F, G. Fraction of Ca^{2+} that is distributed between calcium buffers (yellow), PMCA pumps (blue) and mitochondria (red) for the three Ca^{2+} loads. Ca^{2+} is initially bound by buffers, but then unloaded by PMCA pumps, but for the largest influx, some accumulates in the mitochondria.

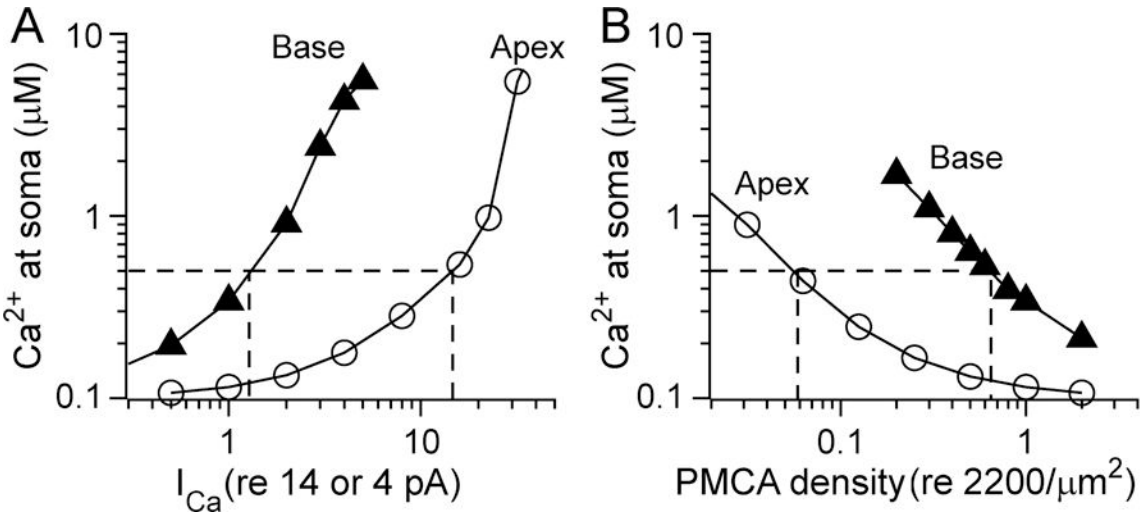

Fig. 6.

Modeling of Ca^{2+} homeostasis in apical and basal OHCs. A. $[Ca^{2+}]$ at the soma as a function of varying the Ca^{2+} current (I_{Ca}) for low-frequency apical OHC (open circles) and high frequency basal OHC (filled traingles). I_{Ca} is plotted on the abscissa, scaled to a standard value of 4 pA (low-frequency apex) and 14 pA (high-frequency base). B. $[Ca^{2+}]$ at the soma as a function of varying PMCA density, scaled to its standard value of 2000/μm^2, distributed over a bundle area of ratio of ~4:1 for low-frequency to high-frequency region. In all cases, the $[Ca^{2+}]$ at the soma increases with larger Ca^{2+} currents (i.e. load) and with smaller PMCA density. However, high-frequency basal OHCs are much more susceptible to changes in these parameters. In both (A) and (B), dashed lines indicate the threshold $[Ca^{2+}]$ 0f 0.5 μM at which mitochondria will start to take up Ca^{2+} (Xu et al., 1997)

TABLE 1.

Model parameters

MET Channel	whole cell Ca^{2+} current	14 pA base, 4.0 pA apex	(Johnson et al., 2011)
Fixed buffer[1]	Concentration	1 mM (stereocilia)	(Xu et al., 1997)
	dissociation coefficient	10 μM	
	forward binding rate	10^7 $M^{-1}s^{-1}$	
Oncomodulin CalbindinD28k	Concentration[2] (mM)	4 mM (apex) 6 mM (base)	(Hackney et al., 2005)
	dissociation coefficient	0.5 μM	(Lee et al., 2000)
	forward binding rate[3]	2×10^7 $M^{-1}s^{-1}$	(Nagerl et al., 2000)
	diffusion coefficient	50 $\mu m^2/s$	(Schmidt et al., 2003)
PMCA	max. velocity of transport[4]	2.0 $\mu mol/m^2s$	(Beurg et al., 2010)
	dissociation coefficient	0.5 μM	(Carafoli et al., 1994)
Mitochondria Uniporter MCU	transport rate[5]	114 mM/s	(Wingrove et al., 1984)
	dissociation coefficient	40 μM	(Xu et al., 1997)
Mitochondria NCX	transport rate	1.8 mM/s	(Patterson et al., 2007)
	dissociation coefficient	5 μM	(Hilgemann et al., 1991)

[1] Fixed buffer values are assumed based on ranges in different neuronal Ca^{2+} models. Ca^{2+} binding ratio, (total buffer concentration)/K_{Ca} =100:1 (Tucker & Fettiplace 1995)

[2] This is the density of the Ca-binding sites, not the density of the molecules

[3] This parameter value was unavailable for oncomodulin so value for calbindinD28k used instead.

[4] 2.0 $\mu mol/m^2s$ = (2000 pumps/μm^2)×(600 ions/pumps/2) /(6.0×10^{23}ions/mol)

[5] This value is derived from Wingrove et al..(1984) Flux, J = 4 nmol/mg/min at C = 0.5 μM.